Hindawi
Adsorption Science & Technology
Volume 2023, Article ID 5716199, 13 pages
https://doi.org/10.1155/2023/5716199

Research Article

Adsorption-Reduction Behavior of Cr(VI) by Ferrihydrite-Fulvic Acid Complexes with Different C/Fe Mole Ratios

Yangyang Zhang,[1,2,3] **Yuxin Chen**,[1] **Junwen An**,[1] **Xiaofei Zhao**,[1,2,3] **and Bo Zu**[1]

[1]*College of River and Ocean Engineering, Chongqing Jiaotong University, Chongqing 400074, China*
[2]*Chongqing Bureau of Geology and Mineral Resources, Chongqing 401121, China*
[3]*Chongqing Gangli Environmental Protection Co., LTD, Chongqing 400042, China*

Correspondence should be addressed to Bo Zu; culangg@gmail.com

Received 8 May 2023; Revised 24 August 2023; Accepted 25 August 2023; Published 6 September 2023

Academic Editor: Chinenye Adaobi Igwegbe

Ferrihydrite and fulvic acid are prevalent components of soils and can significantly influence the environmental behavior of Cr(VI) in these matrices. Prior research has investigated the sorption behavior of Cr(VI) by ferrihydrite and fulvic acid independently; however, the sorption-reduction capacity of Cr(VI) by the ferrihydrite-fulvic acid complex, which is ubiquitously present in soils, has been less explored. In this study, ferrihydrite-fulvic acid complexes (Fh-FA) with varying C/Fe mole ratios were synthesized, and the adsorption-reduction behaviors of Cr(VI) on Fh-FA were examined using batch experiments, FTIR, BET, XRD, SEM-EDS, and XPS. The results demonstrate that the pseudo-second-order kinetic model can accurately describe the adsorption process of Fh-FA on Cr(VI), which can be delineated into three stages: rapid adsorption (0-30 min), slow adsorption (30-120 min), and reaction equilibrium (>120 min). The adsorption of Cr(VI) on Fh-FA primarily occurs through chemisorption. FTIR and XPS analyses revealed that Cr(VI) is initially adsorbed by Fe-OH on the Fh-FA surface. However, as the C/Fe mole ratio of Fh-FA increases, more Fe-OH is complexed by -COOH from FA, resulting in a decrease in the adsorption capacity of Cr(VI) by Fh-FA. The number of phenolic hydroxyl groups from FA also increases, providing additional electrons to reduce Cr(VI) to Cr(III) with increasing C/Fe mole ratio. This study not only emphasizes the adsorption-reduction behavior of Cr(VI) by ferrihydrite-fulvic acid complexes but also uncovers the interplay between C/Fe mole ratios and Cr(VI) adsorption-reduction, contributing to a more comprehensive understanding of the relative roles of Fe hydroxides and natural organic matter in soil environments. These findings have significant implications for Cr(VI) management in soils, enhancing our capability to protect and sustain the environmental quality.

1. Introduction

China is the world's foremost producer of chromium chemicals, with annual chromium production accounting for over 50% of global output. This leads to the accompanying issue of significant chromium soil pollution, a challenge that is increasingly prominent in environmental protection efforts within the nation [1, 2]. As China continues to strengthen its environmental protection requirements, numerous chromium-related enterprises have closed, leaving chromium-containing waste dumps as the country's primary chromium pollution sites [3, 4]. These sites, with high concentrations of Cr(VI) in their soils, pose a severe threat to surrounding ecological environments and urgently necessitate soil remediation [5].

The chemical reduction method [6] is commonly employed to remediate Cr(VI)-contaminated soil, with the critical process involving the conversion of highly toxic Cr(VI) to Cr(III) precipitate via reduction reactions using reducing agents such as $FeSO_4$ [6, 7], Fe^0 [8–10], and CaS_4 [11–13]. This method effectively diminishes the migration ability and bioavailability of Cr(VI). However, this approach has sparked concerns over the potential secondary pollution caused by the excessive reductants added to the soil. In response, researchers have begun to examine essential natural minerals [11, 14–16] and organic matter [17–20] that can

adsorb-reduce Cr(VI), offering a potentially more sustainable and less polluting remediation method.

Ferrihydrite (Fh) is a typical weakly crystalline trivalent iron hydroxide abundant in soil environments and serves as an important precursor to other secondary iron oxides with superior crystalline structures [21]. Due to its large specific surface area and high surface activity, Fh influences the migration and transformation of pollutants in the environment through adsorption and coprecipitation, making it a key soil mineral for heavy metal interaction. The adsorption of Cr(VI) on Fh has been extensively investigated [22, 23]. Zhu et al. [24] discovered that under acidic conditions, Fh could adsorb Cr(VI) at levels reaching 40-50 mg/g. Mamun et al. [25] found that the removal of Cr(VI) by artificially prepared Fh occurred through co-precipitation. Fh rarely exists as a pure mineral in natural environments and typically coprecipitates with organic matter at interfaces with soil, sediment, and aqueous solutions, forming Fh-organic matter complexes [26, 27].

Most current research on Fh-organic matter complexes focuses on Fh-humic acid complexes [28–31]. Wang et al. [32] determined that under weakly acidic conditions, the equilibrium adsorption of Cr(VI) by Fe(III)-HA coprecipitation was lower than that of the pure iron oxide. Yu et al. studied the reaction of Fe_3O_4-HA complex with Cr(VI) following the "adsorption-reduction-complexation" mechanism [28]. Fulvic acid (FA) is another common soluble organic matter found in terrestrial and aquatic environments. Owing to its abundant reactive functional groups, such as carboxyl, phenolic hydroxyl, and hydroxyl groups, it can act as an electron shuttle to promote metal ion reduction and can complex with metals, playing a crucial role in limiting heavy metal migration [33–35]. As another vital component of humus, FA has a lower molecular weight and more functional groups than humic acid. However, the impact of its complex with Fh on the migration and transformation of Cr(VI) is seldom reported, and the adsorption mechanism remains unexplored.

Given this background, the present study is aimed at filling this critical void in our understanding. Specifically, our objectives are threefold: To determine the structure and microstructure of Fh-FA complexes as their C/Fe mole ratio increases. To ascertain the adsorption-reduction characteristics of Cr(VI) on Fh-FA complexes. To illustrate the removal mechanism of Cr(VI) by Fh-FA complexes. Through laboratory batch sorption experiments, characterization, and analytical tools, we compare the Cr(VI) removal efficiencies of Fh and Fh-FA complexes under various conditions. This investigation stands to provide theoretical support for developing efficient remediation methods for Cr(VI)-contaminated soils with minimal secondary contamination, thus offering a crucial step forward in addressing the global challenge of chromium soil pollution.

2. Materials and Methods

2.1. Preparation of Fh and Fh-FA Complexes. Ferrihydrite (Fh) was prepared using the method described by Schwetmann and Cornell for the synthesis of 2-line Fh [36]. A total of 40.40 g of $Fe(NO_3)_3{\cdot}9H_2O$ was weighed and dissolved in 500 mL of deionized water in a beaker. Under vigorous stirring, 1 mol/L NaOH was slowly added until the pH reached approximately 7.0. The resulting suspension was then centrifuged at 6,000 rpm for 10 minutes. The precipitate was repeatedly washed with deionized water (3-5 times) to remove excess salt ions and then freeze-dried.

The Fh-FA complex preparation was adapted from Wang et al. [32] and Chen [37] et al. with minor modifications. Initial C/Fe mole ratios were set to 0.5, 1.0, and 1.5 (Fh-FA0.5, Fh-FA1.0, and Fh-FA1.5); these C/Fe molar ratios were set to represent the typical conditions in natural environments [38–40]. Differences in C/Fe mole ratios were achieved by adjusting the mass of fulvic acid (FA). The pH of the solution was maintained at 5.0 ± 0.1 during the complexation process to simulate the weak acidic environment commonly found in contaminated soils. A specific amount of FA (Sinopharm Chemical Reagent Co., Ltd.) was dissolved in a beaker using 1 mol/L NaOH under vigorous stirring. Subsequently, 4.04 g of $Fe(NO_3)_3{\cdot}9H_2O$ was dissolved in 50 mL of deionized water and mixed with the target FA concentration solution. The pH was adjusted to 6.0 ± 0.1 using 1 mol/L NaOH under vigorous stirring and stirred continuously in the dark for 1 hour, followed by shaking for 24 hours. Finally, the suspensions were centrifuged at 3,500 rpm for 5 minutes, and the solid was washed with deionized water three times. The precipitate was freeze-dried, gently ground to pass through a 100-mesh sieve, and stored in sealed brown glass bottles before use.

2.2. Characterization of Fh and Fh-FA Complexes. The surface area of each sample was determined using the Brunauer-Emmett-Teller (BET) method (Quantachrome-EVO). Scanning electron microscopy-energy dispersive energy dispersive spectroscopy X-ray spectroscopy (SEM-EDX, ZEISS Sigma 300) was employed to observe the morphology and surface element distribution of Fh-FA complexes with different C/Fe mole ratios. X-ray diffraction (XRD, Rigaku Ultima IV) in the range of 15-70° was used to confirm the crystal structures of the prepared materials with different C/Fe mole ratios of Fh-FA complexes. Fourier-transform infrared (FT-IR) spectroscopy (Thermo Scientific Nicolet iS20) in the range of 4,000-400 cm^{-1} was used to characterize the surface functional groups of the Fh-FA complexes. X-ray photoelectron spectroscopy (XPS, Thermo Scientific K-Alpha) was employed to study the elemental content and chemical states of the Fh-FA complexes, with X-ray excitation provided by a monochromatic Al Kα source (excitation energy 1486.6 eV). The binding energies of the spectra were corrected using the hydrocarbon component of adventitious carbon at 284.8 eV. XPS data fitting was performed using XPSPEAK 41. The carbon content of the Fh-FA samples was ascertained using a Vario Micro Cube CHNS analyzer. To determine the Fe content, approximately 2 mg of Fh-FA samples were dissolved in 5 mL of 36% HCl. This solution was then diluted to a final volume of 30 mL with 1% (v/v) HCl. The concentrations of Fe were measured using ICP-OES. Data processing and plotting were carried out using Excel 2020 and Origin 2023.

2.3. Batch Experiments. Batch sorption studies were conducted at varying pH, reaction times (3-180 min), and adsorbate concentrations (10-180 mg/L) to determine the kinetics and obtain equilibrium isotherms. All batch experiments were carried out in 20 mL glass vials, with 20 mg of Fh or Fh-FA added to each vial, followed by the addition of 20 mL of 50 mg/L Cr(VI) solution. For the thermodynamics study, the Cr(VI) concentrations were systematically varied, including values of 10, 30, 50, 70, 90, 120, 150, and 180 mg/L. $NaNO_3$ (10 mM) was used as the background electrolyte because Na^+ is one of the most abundant cations in soil [41]. In the experiment investigating the impact of pH on adsorption, three distinct pH levels were employed, specifically 3, 5, and 7. During the kinetic and thermodynamic studies, a pH of 5 was utilized, reflecting its status as a common pH level found in soil. The pH of the Cr(VI) solutions was adjusted using 0.01 M HNO_3 and NaOH. To ensure complete mixing, each sample was shaken at 20°C using an incubator shaker with an agitation speed of 200 rpm, with all experiments performed in triplicate. At predetermined time intervals, a batch of flasks was removed, followed by vacuum filtration using a 0.45 μm membrane. The concentration of Cr(VI) in the filtrate was determined using a UV/Vis spectrophotometer at 540 nm after reacting with diphenylcarbazide.

To differentiate between Cr(VI) and Cr(III) on Fh-FA, a 0.1 M ($NaOH+Na_2SO_4$) solution was used as a desorption solution to desorb Cr(VI) from Fh-FA for 24 hours. Due to the competitive adsorption of OH^- to $HCrO_4^-$, it was inferred that a high concentration of OH^- could replace nearly all adsorbed Cr(VI) on Fh-FA. The content of Cr(III) on Fh-FA was calculated from the difference between the total Cr and Cr(VI) content on Fh-FA.

2.4. Data Analysis. The total removal (Q_T), total adsorption (Q_{ad}), and total reduction (Q_{re}) of Cr(VI) on the complex were calculated as follows:

The total removal of Cr(VI) by the complex (Q_T) was determined using the equation:

$$Q_T = (C_0 - C_t) \cdot \frac{V}{m}, \quad (1)$$

where Q_T represents the Cr content on Fh-FA (mg/g), C_0 is the initial concentration of Cr(VI) in solution (mg/L), C_t is the residual concentration of Cr(VI) in solution at time t (mg/L), V is the volume of the Cr(VI) solution (20 mL), and m is the mass of Fh-FA (20 mg).

Two forms of Cr were present on magnetite: adsorbed Cr(VI) (Q_{ad}) and reduced Cr(III) (Q_{re}). The content of reduced Cr(III) was calculated from the difference between Q_T and Q_{ad}.

$$Q_{re} = Q_T - Q_{ad}, \quad (2)$$

where Q_{ad} represents the content of adsorbed Cr(VI) on Fh-FA (mg/g) and Q_{re} is the content of reduced Cr(III) on Fh-FA (mg/g).

3. Results and Discussion

3.1. Characterization of Fh-FA Complexes. The BET analysis revealed that the specific surface areas of Fh, Fh-FA0.5, Fh-FA1.0, and Fh-FA1.5 were 36.97, 3.40, 2.08, and 1.03 m^2/g, respectively. The specific surface area of the Fh-FA complex decreased gradually as the amount of FA increased. This could be attributed to FA coating a portion of the mineral surface, leading to a reduced specific surface area of the Fh-FA complex. Alternatively, it could result from the coprecipitation of Fh and FA, where the addition of FA causes the complex to form a denser agglomerate, leading to a decrease in the specific surface area.

A similar observation has been reported in the study by Du et al. [42] regarding Fh-OM coprecipitates. Their research found that coprecipitation results in substantial coverage or occlusion of the Fh surface. The significant decrease in specific surface area also implies reduced N_2 sorption, indicating the blockage of pores and the formation of aggregates inaccessible to N_2. Due to the solubility of FA, not all FA coprecipitates with Fh. We have analyzed the C and Fe content of the Fh-FA complex. The results show that the actual C/Fe molar ratios in Fh-FA 0.5, Fh-FA 1.0, and Fh-FA 1.5 are 0.49, 0.98, and 1.45, respectively.

XRD results (Figure 1(a)) indicated that Fh does not display very sharp peaks, with only two relatively broad, weak-intensity peaks appearing at 2θ of 35° and 62°. When comparing the Fh-FA complexes with different C/Fe mole ratios, the shape and position of the diffraction peaks before and after FA and Fh combination are similar to those of Fh, and no new diffraction peaks emerge. This suggests that no new crystal structure forms after the combination of FA and Fh, and the addition of FA does not damage the original crystal structure of Fh.

In the FT-IR spectrum of FA (Figure 1(b)), absorption peaks corresponding to -OH vibration (3400 cm^{-1}), C-H vibration (2926 cm^{-1}), -COOH (1628 cm^{-1}) vibration, phenolic-OH bending vibration (1384 cm^{-1}), and hydroxyl C-O vibration (1046 cm^{-1}) were found [43–45]. In the FTIR spectrum of Fh, Fe-OH bending vibration (837 cm^{-1}) and hydrogen bond-OH stretching vibration (3400 cm^{-1}) peaks were identified [46]. The Fh-FA complex displayed peaks at 837, 1035, 1230, 1384, 1600, and 3400 cm^{-1}, all of which originate from Fh and FA. It is worth noting that the phenolic hydroxyl O-H bending vibration (1380 cm^{-1}) peaks gradually increase with the C/Fe mole ratio, and the increasing FA content in Fh-FA complexes raises their surface phenolic hydroxyl concentration. However, the peak intensity of the -COOH vibration (~1628 cm^{-1}) of the three Fh-FA complexes did not exhibit significant changes, likely because the surface binding of FA to Fh is mainly achieved through the complexation of -COOH from FA with -OH from Fh. SEM images (Figures 1(c)–1(f)) showed that the Fh surface is rough, cracked, and furrowed, without a consistent morphology. As FA is added and the C/Fe mole ratio changes, the complex surface becomes increasingly rough, with more irregular flake-like particles.

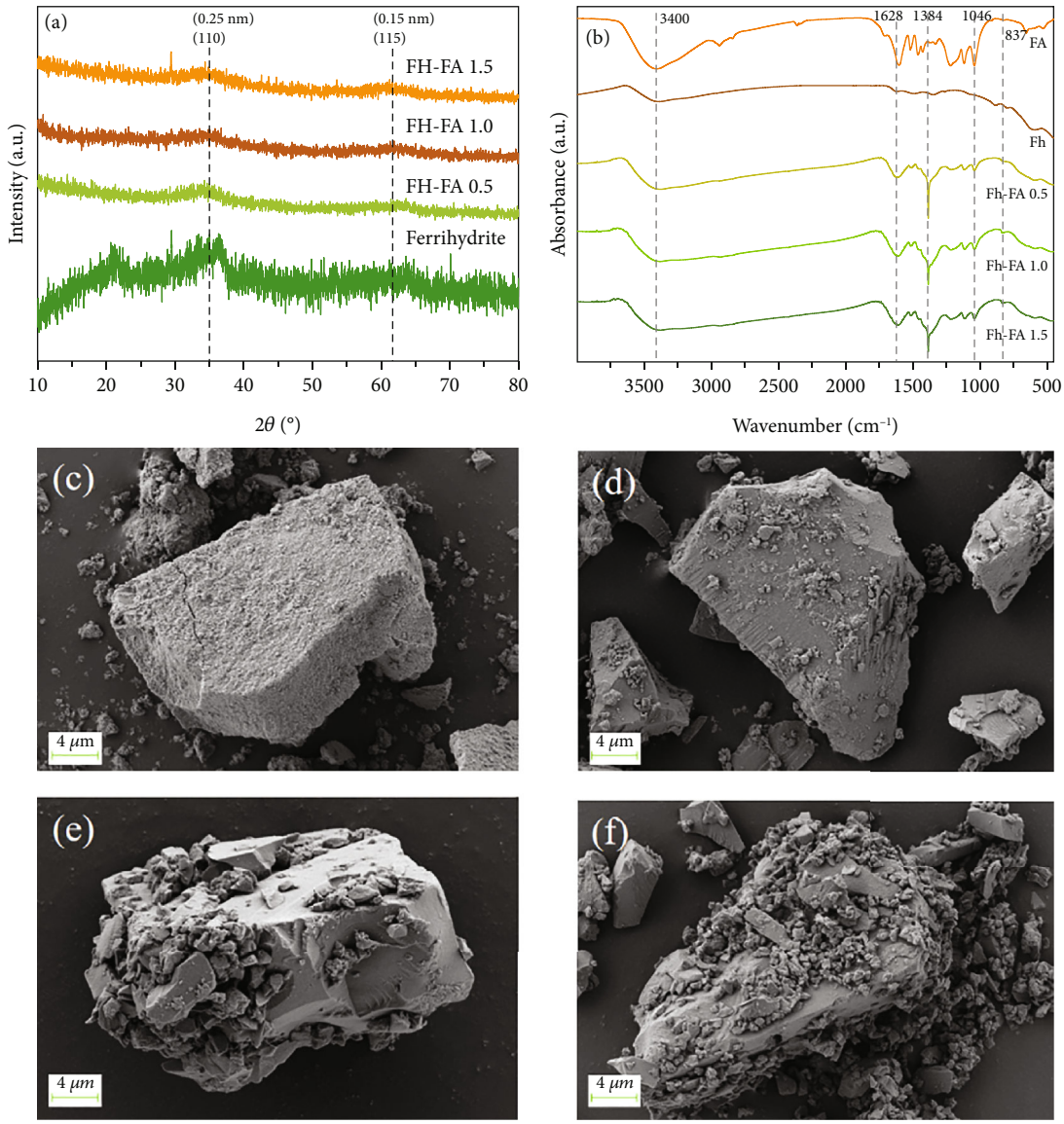

Figure 1: XRD (a), FTIR (b) of Fh and Fh-FA samples, SEM of Fh (c), Fh-FA0.5 (d), Fh-FA1.0 (e), and Fh-FA1.5 (f).

3.2. Effect of pH on Adsorption of Cr(VI) by Fh-FA Complexes. The efficiency of Cr(VI) adsorption is significantly affected by the pH level. We established three distinct pH conditions: 3, 5, and 7, to examine the influence of external environmental changes on the adsorption behavior of Cr(VI). As depicted in Figure 2(a), the adsorption capacity of all complexes for Cr(VI) diminishes with an increase in pH. Under the acidic condition of pH 3, all Fh-FA complexes exhibit the highest adsorption capacity for Cr(VI), with the corresponding adsorption capacities of Fh, Fh-FA 0.5, Fh-FA 1.0, and Fh-FA 1.5 being 6.74 mg/g, 5.81 mg/g, 4.68 mg/g, and 4.24 mg/g, respectively. Conversely, under the mildly acidic and neutral conditions of pH 5 and 7, the change in the adsorption capacity of the Fh-FA complexes for Cr(VI) is not significant, but the adsorption capacity in the neutral environment of pH 7 is relatively lower, with corresponding adsorption capacities of 3.94 mg/g, 3.52 mg/g, 3.19 mg/g, and 2.97 mg/g. In summary, acidic environments are more favorable for the adsorption and removal of Cr(VI) by Fh-FA complexes. The primary reason is that within the pH range of 3-7, Cr(VI) predominantly exists as $HCrO_4^-$ and CrO_4^{2-}. From the zeta potential results (Figure 2(b)), it is evident that the zeta potential of the Fh-FA complexes decreases with an increase in both pH and the C/Fe ratio. This decrease can be attributed to the electrostatic repulsion, which in turn reduces the adsorption capacity of the Fh-FA complexes for Cr(VI) as the pH increases. Under the same pH conditions, it was observed that as the FA content in the Fh-FA complex increased, the adsorption capacity for Cr consistently decreased. This phenomenon closely aligns with the concomitant reduction in the BET surface area of the Fh-FA complex in relation to the escalation in FA content. Generally, a larger specific surface area is conducive to the physical adsorption of metal ions by soil minerals or soil organic matter. As such, this research posits that the physical adsorption of Cr(VI) may be present on the

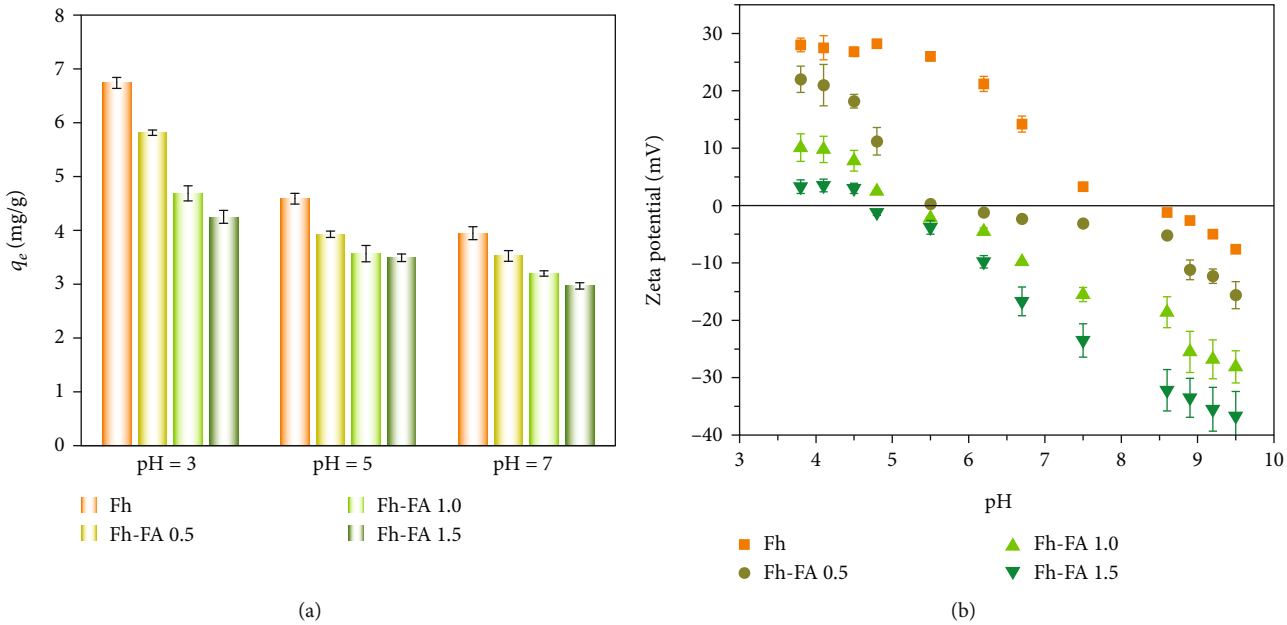

Figure 2: (a) Effect of pH on adsorption of Cr(VI) by Fh-FA complexes and (b) zeta potential of Fh and Fh-FA complexes. Experimental condition: Cr(VI) concentration = 50 mg/L, T = 25°C, pH = 3, 5, and 7, dose = 0.8 g/L, reaction time = 240 min, and I = 10 mM $NaNO_3$.

complex surface, with BET serving as one of the main governing factors in the control of adsorption quantity.

3.3. Kinetics of Cr(VI) Adsorption and Reduction by Fh-FA. The adsorption and reduction process of Cr(VI) by Fh-FA complexes with varying C/Fe mole ratios can be categorized into three stages: rapid adsorption stage, slow adsorption stage, and reaction equilibrium stage (Figure 3). The adsorption of Cr(VI) by Fh-FA complexes with different C/Fe mole ratios is relatively quick within the first 30 minutes, reaching approximately 80% of the maximum adsorption capacity. Between 30 and 120 minutes, the adsorption rate of Cr(VI) progressively declines, and the equilibrium adsorption quantity of Cr(VI) increases marginally, with the adsorption process eventually stabilizing after 120 minutes. This suggests that the adsorption of Cr(VI) by the Fh-FA complex primarily occurs during the initial two stages of the reaction.

As shown in Figures 3(b) and 3(c), the equilibrium adsorption amount of Fh in the reaction with Cr(VI) was 4.5 mg/g; however, Fh did not reduce Cr(VI). This indicates that Fh removes Cr(VI) via adsorption, potentially due to its high specific surface area of 36.97 m^2/g and numerous positively charged adsorption sites. As the C/Fe mole ratio increases, the adsorption of Fh-FA on Cr(VI) gradually decreases for three reasons: (1) an increase in the C/Fe mole ratio causes FA to reduce the specific surface area and pore capacity of the complex, rendering it less favorable for Cr(VI) adsorption through physical effects such as electrostatic attraction; (2) FTIR results demonstrate that the -COOH group complexes with Fh-OH, reducing adsorption sites on the Fh surface, which is unfavorable for Cr(VI) adsorption via chemical interactions like ligand exchange; and (3) the presence of numerous acidic functional groups, such as carboxyl groups, in FA renders it prone to negative charging under acidic conditions and creates strong electrostatic repulsion against Cr anions. Consequently, greater FA content in Fh-FA results in lower Cr(VI) adsorption capacity.

With an increasing C/Fe mole ratio, the reduction of Cr(VI) by Fh-FA gradually rises (Figure 3(c)). FA contains a significant number of reducing functional groups, such as phenolic hydroxyl and hydroxyl groups (Figure 1(b)), which can serve as electron donors to facilitate Cr(VI) reduction [21]. As a result, the reduction capability of Fh-FA for Cr(VI) is positively correlated with the FA amount in the Fh-FA complex. These findings imply that both Fh and FA contribute to the adsorption and reduction of Cr(VI), with Fh providing surface sites for Cr(VI) adsorption and FA supplying electrons for Cr(VI) reduction.

Figure 3(d) presents the percentage ratio of the adsorbed and reduced Cr(VI) under different reaction time conditions. It can be observed that at equilibrium, 34.8%, 39.9%, and 46.1% of Cr(VI) on the surfaces of Fh-FA 0.5, Fh-FA 1.0, and Fh-FA 1.5, respectively, have been reduced, with the reduction amounts being 1.30 mg/g, 1.39 mg/g, and 1.50 mg/g, respectively. Fh-FA 0.5 and Fh-FA 1.0 essentially completed the reduction of Cr(VI) on their surfaces at the initial stages of the reaction, and the percentage of Cr(VI) reduction did not change significantly with the extension of reaction time. However, the reduction percentage of Cr(VI) by Fh-FA 1.5 was 61.6% at 3 minutes of reaction, which decreased to 46.1% as the reaction proceeded to 240 minutes. This could be because Fh-FA 1.5, compared to Fh-FA 0.5 and Fh-FA 1.0, contains a higher amount of FA and more phenolic hydroxyl groups on its surface. Therefore, at the beginning of the reaction, it can reduce the adsorbed Cr(VI) on its surface to Cr(III). However, as the reaction proceeds, the number of phenolic hydroxyl groups

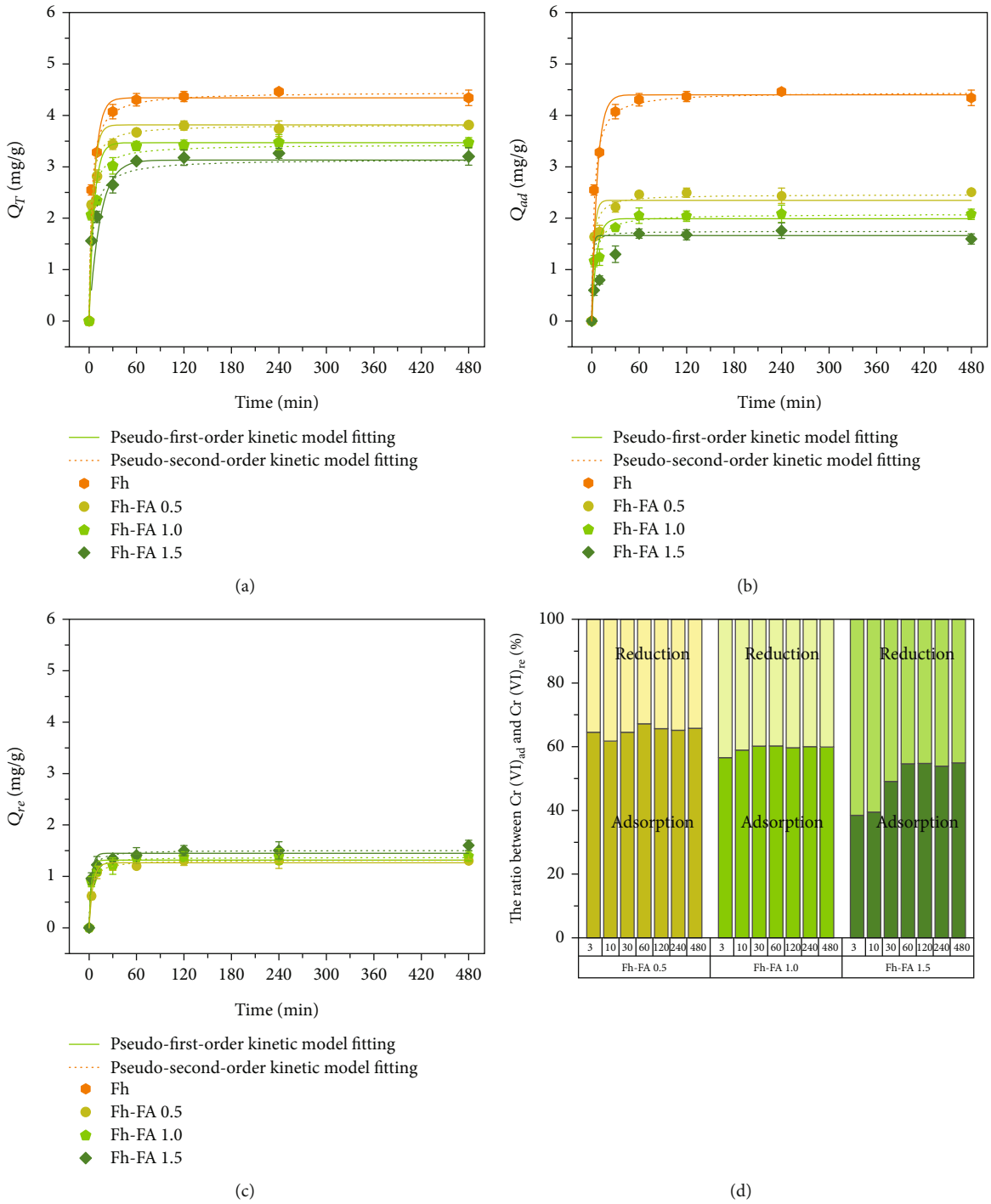

FIGURE 3: Kinetic fitting of (a) total Cr(VI) removal, (b) total Cr(VI) adsorption, and (c) total Cr(VI) reduction and (d) the ratio between the adsorbed Cr(VI) and reduced Cr(VI) by Fh-FA complexes with different C/Fe mole ratios. Experimental condition: Cr(VI) concentration = 50 mg/L, T = 25°C, pH = 5, dose = 0.8 g/L, reaction time = 3, 10, 30, 60, 120, 180, 240, and 480 min, I = 10 mM $NaNO_3$.

that can provide electrons decreases, weakening its reduction ability, and the already reduced Cr(III) may be partially oxidized back to Cr(VI).

To quantitatively describe the kinetic processes of Cr(VI) adsorption and reduction by complexes with varying C/Fe mole ratios, the experimental results were fitted using pseudo-first-order and pseudo-second-order kinetic models. The fitted outcomes are displayed in Table 1. Comparing the fitted effect plots and parameters reveals that the correlation coefficient R^2 for the pseudo-second-order kinetic model is greater than that for the pseudo-first-order kinetic model, indicating that the pseudo-second-order kinetic model is

Table 1: Calculated kinetics parameters for total Cr(VI) removal, total Cr(VI) adsorption and total Cr(VI) reduction by Fh-FA complexes.

C/Fe mole ratio	Pseudo-first-order kinetic model			Pseudo-second-order kinetic model		
	q_m/(mg/g)	K_1/min^{-1}	R^2	q_m/(mg/g)	K_2/(g/(mg-min))	R^2
Q_T						
Fh	4.4003	0.1450	0.76097	4.4538	0.0734	0.9551
Fh-FA0.5	3.7729	0.1987	0.79632	3.8161	0.1171	0.9799
Fh-FA1.0	3.3755	0.1556	0.61231	3.4309	0.1038	0.8670
Fh-FA1.5	3.1312	0.0716	0.53659	3.1494	0.0745	0.9147
Q_{ad}						
Fh	4.3625	0.2889	0.8410	4.4915	0.1394	0.9731
Fh-FA0.5	2.3486	0.3249	0.5392	2.4594	0.1984	0.8244
Fh-FA1.0	1.9914	0.1615	0.6617	2.0803	0.1338	0.8550
Fh-FA1.5	1.6647	0.0694	0.8864	1.7643	0.0651	0.9139
Q_{re}						
Fh	—	—	—	—	—	—
Fh-FA0.5	1.3173	0.3417	0.9545	1.3719	0.3968	0.9879
Fh-FA1.0	1.2645	0.2116	0.9905	1.3206	0.2536	0.9932
Fh-FA1.5	0.8968	0.1098	0.925	0.9514	0.1787	0.9743

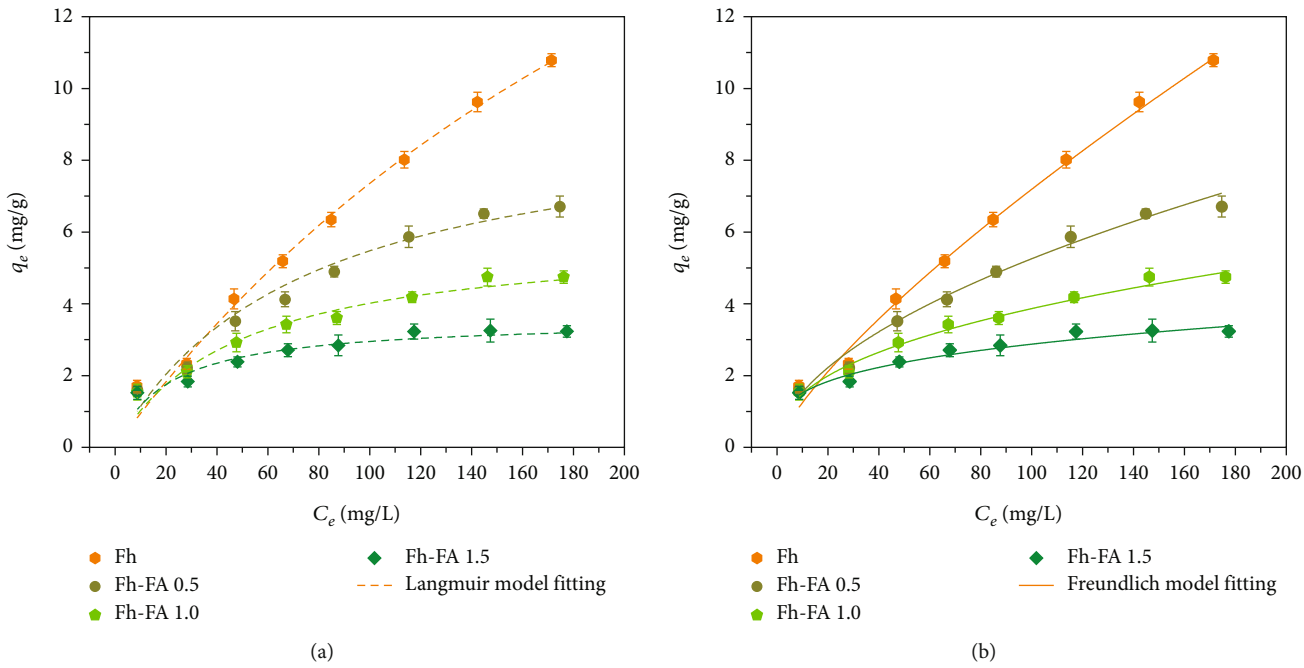

Figure 4: Langmuir isothermal model (a) and Freundlich isothermal model (b) for Cr(VI) adsorption by Fh-FA complexes. Experimental condition: Cr(VI) concentration = 10, 30, 50, 70, 90, 120, 150, and 180 mg/L, T = 25°C, pH = 5, dose = 0.8 g/L, reaction time = 240 min, and I = 10 mM $NaNO_3$.

better suited to describe the adsorption and reduction processes of Cr(VI) by the complex. This suggests that Cr(VI) adsorption on Fh-FA is predominantly controlled by chemical processes [47–49].

3.4. Thermodynamics of Cr(VI) Adsorption by Fh-FA. Figure 4 demonstrates that the adsorption of Cr(VI) is enhanced by varying C/Fe mole ratios of Fh-FA complexes as the initial concentration of Cr(VI) increases. As the C/Fe mole ratio increases, the equilibrium adsorption of Cr(VI) by Fh-FA 0.5, Fh-FA 1.0, and Fh-FA 1.5 progressively decreases to 10.92, 5.87, and 2.47 mg/g, respectively. The isothermal adsorption behavior of Cr(VI) on Fh-FA complexes was analyzed using Freundlich and Langmuir models, with the fitted results displayed in Table 2. The results indicate that both Langmuir and Freundlich models

Table 2: Langmuir and Freundlich adsorption isotherm model parameters.

Adsorbent	Langmuir model			Freundlich model		
	q_m/(mg/g)	K_L/(L/mg)	R^2	n	K_F/(mg/g)	R^2
Fh	30.39	0.0032	0.99	1.31	0.21	0.99
Fh-FA0.5	9.49	0.0136	0.96	1.86	0.45	0.99
Fh-FA1.0	5.95	0.0207	0.96	2.42	0.58	0.99
Fh-FA1.5	3.56	0.0482	0.88	3.59	0.80	0.95

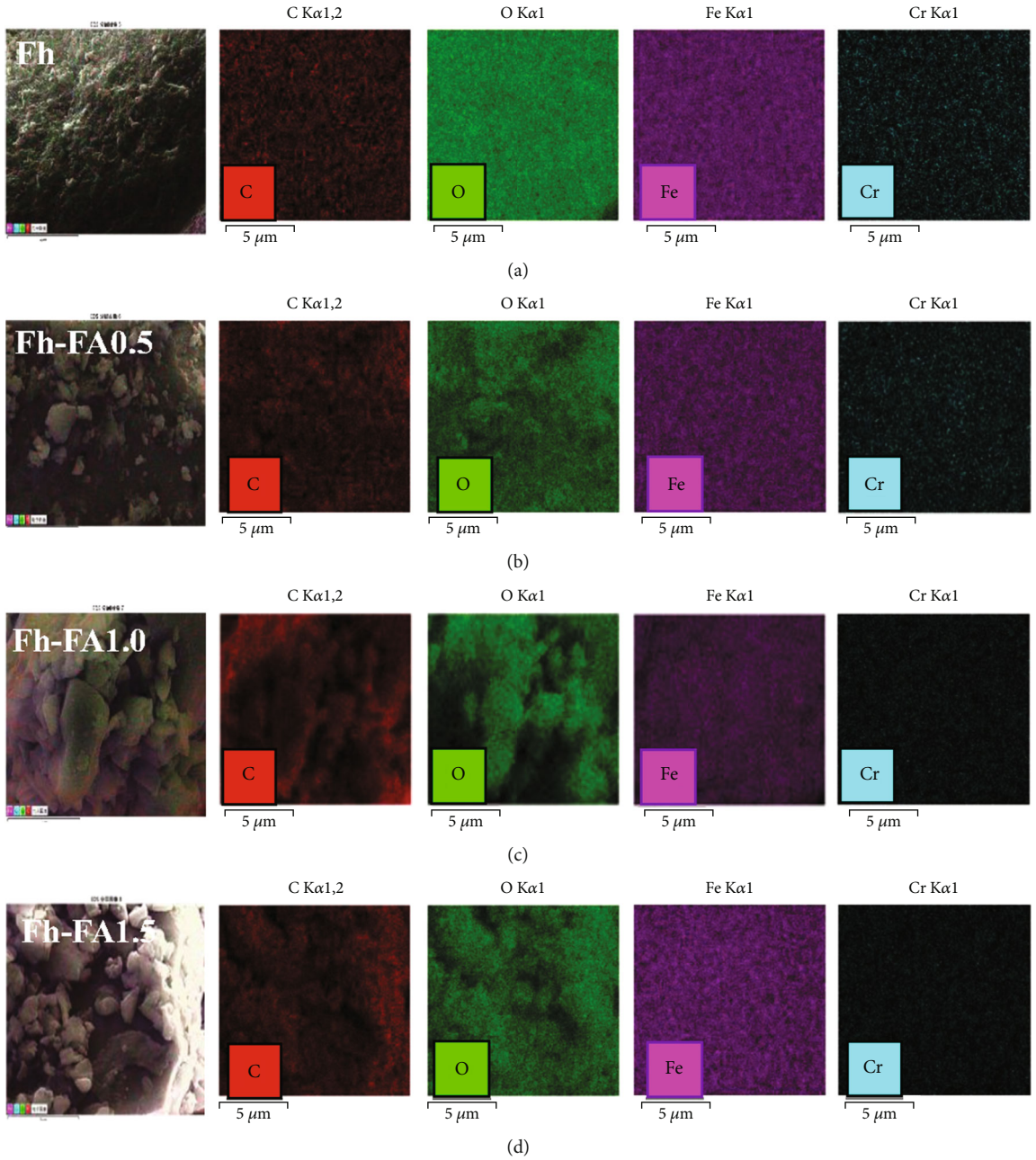

Figure 5: EDS-mapping of Fh (a), Fh-FA0.5 (b), Fh-FA1.0 (c), and Fh-FA1.5 (d) after reaction with Cr(VI).

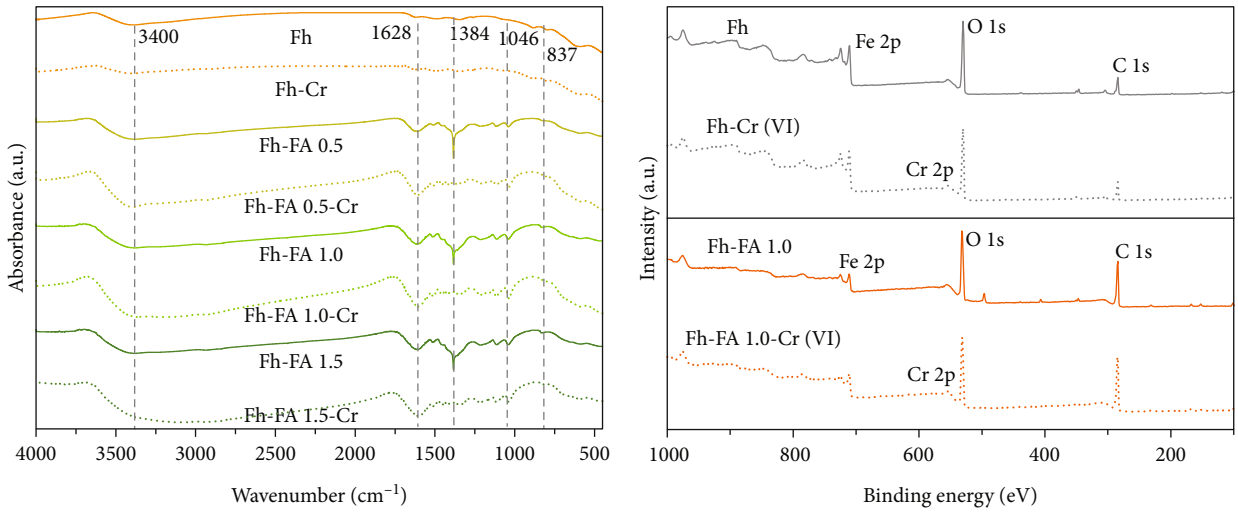

Figure 6: The FT-IR spectra (a) and full XPS spectra (b) of Fh-FA complexes before and after Cr(VI)adsorption. Soild line: before adsorption; dot line: after adsorption.

effectively describe the isotherm data. The Langmuir maximum adsorption capacities of Fh, Fh-FA 0.5, Fh-FA 1.0, and Fh-FA 1.5 for Cr(VI) were 30.39, 9.49, 5.95, and 3.56 mg/g, respectively. These findings are consistent with those obtained from the kinetic analysis, suggesting that the initial concentration of Cr(VI) is positively correlated with the adsorption capacity of the Fh-FA complex on Cr(VI). Additionally, the available adsorption sites on the surface of Fh-FA are the primary factors governing the adsorption capacity.

3.5. Adsorption and Reduction Mechanism of Cr(VI) by Fh-FA Complexes. The EDS mapping (Figure 5) revealed the uniform distribution of C, Fe, and O on the surface of Fh-FA complexes, indicating that FA was loaded onto the Fh surface. The distribution of the Cr signal on the Fh-FA complex surface gradually decreased with increasing C/Fe mole ratio, consistent with the adsorption experiment results.

FTIR spectroscopy of the Fh-FA complexes before and after Cr(VI) adsorption is shown in Figure 6(a). Before Cr(VI) adsorption, Fh-FA complexes displayed absorption peaks at approximately 3400, 1628, 1348, 1046, and 837 cm^{-1}. The peak at 837 cm^{-1} weakened after Cr(VI) adsorption, suggesting the involvement of Fe-OH on the complex surface in Cr(VI) adsorption. The significant weakening of the 1384 cm^{-1} absorption peak indicates the participation of surface phenolic-OH in the reaction. According to other researchers, phenolic-OH is the primary electron donors and participates in Cr(VI) reduction [50–52].

As mentioned earlier, after the complexation of Fh with FA of different concentrations, the intensity of the -COOH vibration peak (~1628 cm^{-1}) of the complex does not show significant changes. This could be attributed to the abundant -COOH present on the surface of FA. The binding of FA to the surface of Fh is primarily achieved through the complexation of -COOH from FA with -OH from Fh. As the concentration of FA in the complex increases, the Fe-OH exposed on the surface of the complex gradually decreases, while the concentration of phenolic hydroxyl groups increases. After the reaction with Cr(VI) is complete, the peak intensity of Fe-OH significantly weakens, and the -COOH peak intensity does not show significant changes. This suggests that Fe-OH is the main functional group adsorbing Cr(VI). The peak intensity of phenolic hydroxyl groups also significantly weakens, indicating that they provide the electrons needed to reduce Cr(VI). The reduction of Cr(VI) increases with the increase in the C/Fe ratio (Figure 3). However, it is noteworthy that the reductive effect produced by the phenolic hydroxyl groups on Cr(VI) is not permanent. As can be discerned from Figure 3(d), although Fh-FA 1.5 can significantly reduce Cr(VI) in the early stages of the reaction, some Cr(III) is reoxidized to Cr(VI) upon exposure to oxygen in the air as the reaction proceeds. Consequently, the identification of a consistent and stable electron donor to maintain the reduced state of Cr(III) is of paramount importance for the remediation of Cr(VI)-contaminated soil.

To further elucidate the Cr(VI) removal mechanism by Fh-FA complexes, X-ray photoelectron spectroscopy (XPS) was performed on complex samples after the reaction to investigate the Cr valence presence on Fh-FA complex surfaces. As shown in Figure 6(b), new peaks corresponding to Cr 2p appeared in the reacted materials when comparing the XPS full spectra of complexes before and after Cr(VI) removal. The XPS spectra of Fh and Fh-FA complexes displayed an insignificant Cr peak at a binding energy of 576.3 eV [53], likely due to the low amount of Cr(VI) adsorbed on the Fh and Fh-FA complex surfaces.

O 1s spectra are shown in Figure 7(a). The O 1s spectra of Fh-FA1.0 before and after Cr(VI) adsorption exhibit -OH (532.67 eV) and Fe-O (530.70 eV) peaks [54, 55]. After adsorption, the Fe-O peak narrowed and its intensity decreased, suggesting the existence of Fe-O-Cr complexation on the Fh-FA complex surface and the crucial role of Fe-O in Cr(VI) adsorption, consistent with the FTIR results. The

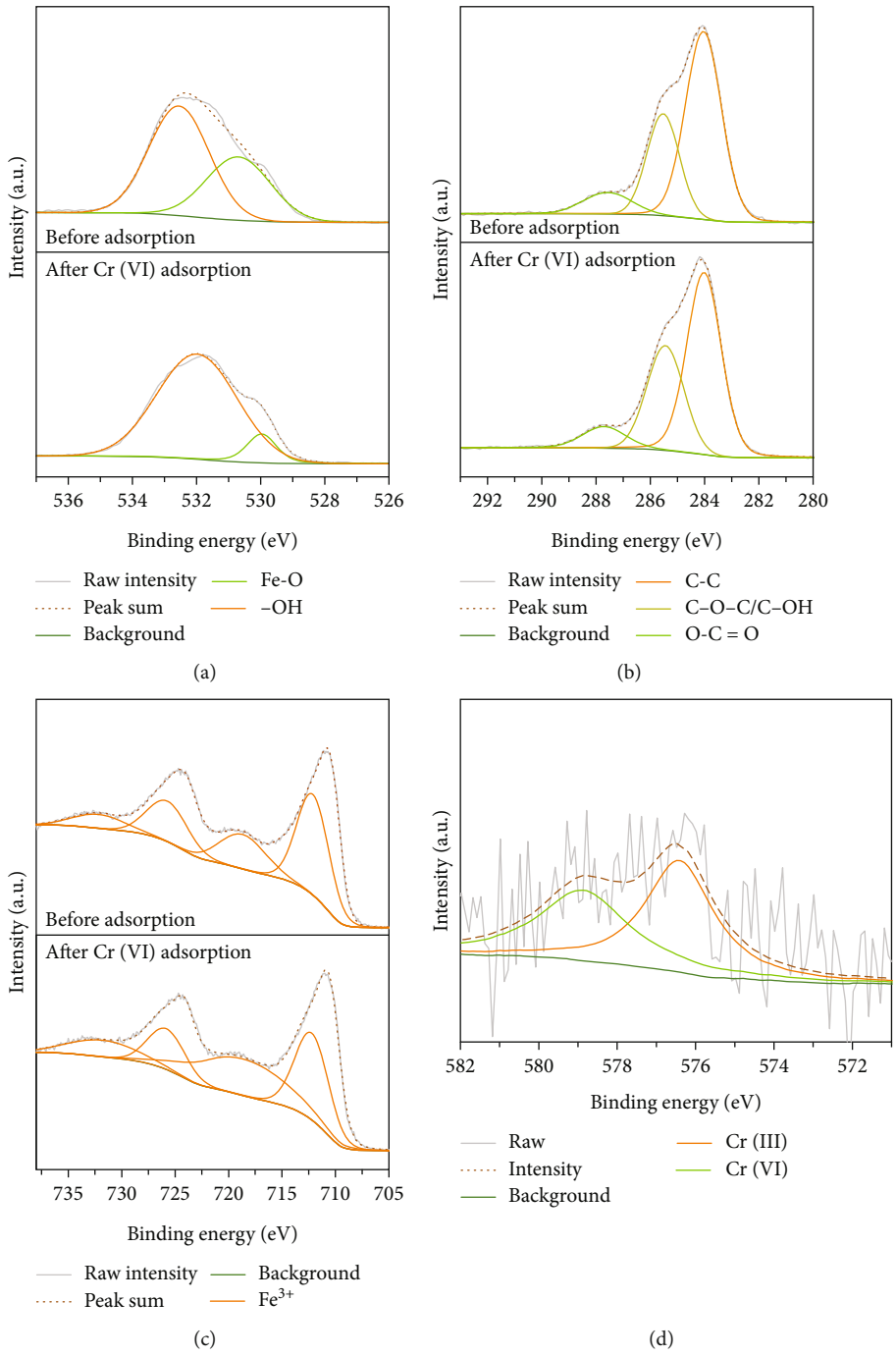

Figure 7: The O 1s (a), C 1s (b), Fe 2p (c), and Cr $2p_{3/2}$ (d). XPS spectra of Fh-FA1.0 before and after absorption.

peak intensity at 532.67 eV in the O1s region increased after adsorption, which according to previous studies [35], can be attributed to the existence of hydroxyl groups in metal hydroxides, such as $Cr(OH)_3$, on the surface of Fh-FA complexes. Other researches [56, 57] also suggest that after Cr(VI) is reduced to Cr(III), Cr(III) predominantly precipitates in the form of $Cr(OH)_3$. Therefore, it is reasonable to believe that, in this study, Cr(III) likely precipitates as $Cr(OH)_3$ on the surface of Fh-FA complexes.

Figure 7(b) shows the C 1s spectra of Fh-FA1.0 before and after Cr(VI) adsorption at 284, 285.8, and 287.6 eV, corresponding to C-C, C-O-C/C-OH, and C=O, respectively [58]. No peak shifts were observed after Cr(VI) removal, and changes in peak proportion were negligible, indicating that Fh-FA complex carbon does not participate in Cr(VI) removal.

Fe 2p spectra before and after Cr(VI) adsorption by Fh-FA1.0 are presented in Figure 7(c). The Fe 2p3/2 peak at 725.7 eV and the Fe 2p1/2 peak at 713.0 eV were ascribed to Fe(III), accompanied by a satellite peak at approximately 720.0 eV [58]. Following adsorption, changes in peak proportion were negligible, signifying that Fe(III) in Fh-FA1.0

was not involved in the Cr(VI) adsorption process. Figure 7(d) displays the Cr 2p3/2 spectrum, with Cr 2p peaks after adsorption at 578.1 and 577.0 eV corresponding to Cr(VI) and Cr(III), respectively. This suggests that a portion of Cr(VI) was reduced by phenolic-OH on the surface of Fh-FA1.0.

4. Conclusion

This study has systematically explored the adsorption-reduction behaviors and mechanisms of Cr(VI) by ferrihydrite-fulvic acid (Fh-FA) complexes. The key findings can be summarized as follows: (1) The Cr(VI) adsorption process by Fh-FA complexes is aptly described by the pseudo-second-order kinetic model, encompassing three stages: rapid adsorption, slow adsorption, and reaction equilibrium. (2) Both Langmuir and Freundlich models fit the isothermal adsorption data, with the Langmuir maximum adsorption capacities decreasing with an increase in the C/Fe ratio. (3) Fe-OH and phenolic-OH played central roles in the Cr(VI) adsorption and reduction, with FTIR and XPS results highlighting the critical mechanism involving Fe-OH, -COOH from FA, and phenolic-OH.

The implications of this research extend beyond the specific parameters investigated, contributing valuable insights into Cr(VI) interactions with iron hydroxides and natural organic matter in soil environments. The observed adsorption and reduction patterns present novel insights that can be leveraged for informed soil remediation strategies, particularly regarding Cr(VI)-contaminated soil. While this study offers a robust analysis of the Cr(VI) behavior on Fh-FA complex surfaces, it also opens avenues for further research. Specifically, the impact of diverse iron hydroxides and the influence of environmental changes on crystal transformation should be explored to provide a more comprehensive understanding of Cr(VI) migration and fate in contaminated soil. In conclusion, this study serves as a significant step forward in understanding Cr(VI) behavior and its implications for soil remediation, enhancing the existing body of knowledge, and offering guidance for future research and practical applications.

Data Availability

The data used to support the findings of this study are included within the article and the supplementary information file.

Conflicts of Interest

The authors declare that they have no known competing financial interests or personal relationships that could have appeared to influence the work reported in this paper.

Authors' Contributions

Yangyang Zhang performed the experiment, funding acquisition, and writing, which includes review and editing. Yuxin Chen did the writing, which includes review and editing. Junwen An contributed to the experiment. Xiaofei Zhao worked on the funding acquisition and writing, which includes review and editing. Zu Bo was responsible for writing, which includes review and editing.

Acknowledgments

This work was supported by the National Natural Science Foundation of China (42207306), Natural Science Foundation of Chongqing, China (cstc2021jcyj-bshX0231), and China Postdoctoral Science Foundation (2022 M720590).

Supplementary Materials

Detailed information on the kinetic and isothermal models can be found in the supplementary information. *(Supplementary Materials)*

References

[1] X. Li, J. Zhang, J. Ma et al., "Status of chromium accumulation in agricultural soils across China (1989-2016)," *Chemosphere*, vol. 256, article 127036, 2020.

[2] B. Chen, M. Wang, M. Duan et al., "In search of key: Protecting human health and the ecosystem from water pollution in China," *Journal of Cleaner Production*, vol. 228, pp. 101–111, 2019.

[3] X. Wang, L. Li, X. Yan, X. Meng, and Y. Chen, "Processes of chromium (VI) migration and transformation in chromate production site: a case study from the middle of China," *Chemosphere*, vol. 257, article 127282, 2020.

[4] J. Wang, X. Hu, T. Shi, L. He, W. Hu, and G. Wu, "Assessing toxic metal chromium in the soil in coal mining areas via proximal sensing: prerequisites for land rehabilitation and sustainable development," *Geoderma*, vol. 405, article 115399, 2022.

[5] L. Xiao, Y. Zhou, J. Ma et al., "The cross-sectional and longitudinal associations of chromium with dyslipidemia: a prospective cohort study of urban adults in China," *Chemosphere*, vol. 215, pp. 362–369, 2019.

[6] Y. Pei, Y. Yang, L. Chen, Y. Yang, and L. Song, "Remediation of chromium-contaminated soil in semi-arid areas by combined chemical reduction and stabilization," *Environmental Pollutants and Bioavailability*, vol. 35, no. 1, article 2157332, 2023.

[7] H. Mou, W. Liu, L. Zhao, W. Chen, and T. Ao, "Stabilization of hexavalent chromium with pretreatment and high temperature sintering in highly contaminated soil," *Frontiers of Environmental Science & Engineering*, vol. 15, no. 4, p. 61, 2021.

[8] W. Yang, X. Li, D. Xi et al., "Synergistic chromium(VI) reduction and phenol oxidative degradation by FeS_2/Fe^0 and persulfate," *Chemosphere*, vol. 281, article 130957, 2021.

[9] C. Zhou, C. Han, X. Min, and T. Yang, "Effect of different sulfur precursors on efficient chromium(VI) removal by ZSM-5 zeolite supporting sulfide nano zero-valent iron," *Chemical Engineering Journal*, vol. 427, article 131515, 2022.

[10] J. Lu, R. Geng, H. Zhang, Z. Yu, T. Chen, and B. Zhang, "Concurrent reductive decontamination of chromium (VI) and uranium (VI) in groundwater by Fe(0)-based autotrophic bioprocess," *Journal of Hazardous Materials*, vol. 452, article 131222, 2023.

[11] T. Wang, W. Wang, Y. Liu, W. Li, Y. Li, and B. Liu, "Roles of natural iron oxides in the promoted sequestration of chromate using calcium polysulfide: pH effect and mechanisms," *Separation and Purification Technology*, vol. 237, article 116350, 2020.

[12] S. Hu, D. Li, Y. Man, Y. Wen, and C. Huang, "Evaluation of remediation of Cr(VI)-contaminated soils by calcium polysulfide: long-term stabilization and mechanism studies," *Science of the Total Environment*, vol. 790, article 148140, 2021.

[13] W. Yuan, W. Xu, Z. Zhang et al., "Rapid Cr(VI) reduction and immobilization in contaminated soil by mechanochemical treatment with calcium polysulfide," *Chemosphere*, vol. 227, pp. 657–661, 2019.

[14] C. Tan, S. Avasarala, and H. Liu, "Hexavalent chromium release in drinking water distribution systems: new insights into zerovalent chromium in iron corrosion scales," *Environmental Science & Technology*, vol. 54, no. 20, pp. 13036–13045, 2020.

[15] T. Zhang, T. Wang, W. Wang, B. Liu, W. Li, and Y. Liu, "Reduction and stabilization of Cr(VI) in soil by using calcium polysulfide: catalysis of natural iron oxides," *Environmental Research*, vol. 190, article 109992, 2020.

[16] K. Ri, C. Han, D. Liang, S. Zhu, Y. Gao, and T. Sun, "Nanocrystalline erdite from iron-rich sludge: green synthesis, characterization and utilization as an efficient adsorbent of hexavalent chromium," *Journal of Colloid and Interface Science*, vol. 608, Part 2, pp. 1141–1150, 2022.

[17] A. Othmani, S. Magdouli, P. Senthil Kumar, A. Kapoor, P. V. Chellam, and Ö. Gökkuş, "Agricultural waste materials for adsorptive removal of phenols, chromium (VI) and cadmium (II) from wastewater: a review," *Environmental Research*, vol. 204, article 111916, Part A, 2022.

[18] Z. Xia, Y. Yang, T. Liu et al., "Chromium biogeochemical cycling in basalt-derived paddy soils from the Leizhou Peninsula, South China," *Chemical Geology*, vol. 622, article 121393, 2023.

[19] O. Enya, N. Heaney, G. Iniama, and C. Lin, "Effects of heavy metals on organic matter decomposition in inundated soils: microcosm experiment and field examination," *Science of the Total Environment*, vol. 724, article 138223, 2020.

[20] X. Fan, S. Ding, M. Chen et al., "Peak chromium pollution in summer and winter caused by high mobility of chromium in sediment of a eutrophic Lake: in situ evidence from high spatiotemporal sampling," *Environmental Science & Technology*, vol. 53, no. 9, pp. 4755–4764, 2019.

[21] J. Yang, X. Xia, J. Liu, J. Wang, and Y. Hu, "Molecular mechanisms of chromium(III) immobilization by organo–ferrihydrite co-precipitates: the significant roles of ferrihydrite and carboxyl," *Environmental Science & Technology*, vol. 54, no. 8, pp. 4820–4828, 2020.

[22] Y. Chen and Z. Li, "Interaction of norfloxacin and hexavalent chromium with ferrihydrite nanoparticles: Synergistic adsorption and antagonistic aggregation behavior," *Chemosphere*, vol. 299, article 134386, 2022.

[23] T. Zhang, B. Tang, and F. Fu, "Influence of montmorillonite incorporation on ferrihydrite transformation and Cr(VI) behaviors during ferrihydrite-Cr(VI) coprecipitates aging," *Science of the Total Environment*, vol. 873, article 162257, 2023.

[24] L. Zhu, F. Fu, and B. Tang, "Coexistence or aggression? Insight into the influence of phosphate on Cr(VI) adsorption onto aluminum-substituted ferrihydrite," *Chemosphere*, vol. 212, pp. 408–417, 2018.

[25] A. A. Mamun, M. Morita, M. Matsuoka, and C. Tokoro, "Sorption mechanisms of chromate with coprecipitated ferrihydrite in aqueous solution," *Journal of Hazardous Materials*, vol. 334, pp. 142–149, 2017.

[26] H. Xu, L. Ji, M. Kong, H. Jiang, and J. Chen, "Molecular weight-dependent adsorption fractionation of natural organic matter on ferrihydrite colloids in aquatic environment," *Chemical Engineering Journal*, vol. 363, pp. 356–364, 2019.

[27] Z. Zhou, E. M. Muehe, E. J. Tomaszewski, J. Lezama-Pacheco, A. Kappler, and J. M. Byrne, "Effect of natural organic matter on the fate of cadmium during microbial ferrihydrite reduction," *Environmental Science & Technology*, vol. 54, no. 15, pp. 9445–9453, 2020.

[28] G. Yu, F. Fu, C. Ye, and B. Tang, "Behaviors and fate of adsorbed Cr(VI) during Fe(II)-induced transformation of ferrihydrite-humic acid co-precipitates," *Journal of Hazardous Materials*, vol. 392, article 122272, 2020.

[29] Q. Xue, Y. Ran, Y. Tan, C. L. Peacock, and H. du, "Arsenite and arsenate binding to ferrihydrite organo-mineral coprecipitate: Implications for arsenic mobility and fate in natural environments," *Chemosphere*, vol. 224, pp. 103–110, 2019.

[30] H. Du, N. Nie, W. Rao, L. Lu, M. Lei, and B. Tie, "Ferrihydrite-organo composites are a suitable analog for predicting Cd(II)-As(V) coexistence behaviors at the soil solid-liquid interfaces," *Environmental Pollution*, vol. 290, article 118040, 2021.

[31] H. Du, C. L. Peacock, W. Chen, and Q. Huang, "Binding of Cd by ferrihydrite organo-mineral composites: Implications for Cd mobility and fate in natural and contaminated environments," *Chemosphere*, vol. 207, pp. 404–412, 2018.

[32] H. Wang, J. Zhang, J. Zhu, J. Chang, N. Wang, and H. Chen, "Synergistic/antagonistic effects and mechanisms of Cr(VI) adsorption and reduction by Fe(III)-HA coprecipitates," *Journal of Hazardous Materials*, vol. 409, article 124529, 2021.

[33] J. Wen, Z. Xue, X. Yin, and X. Wang, "Insights into aqueous reduction of Cr(VI) by biochar and its iron-modified counterpart in the presence of organic acids," *Chemosphere*, vol. 286, article 131918, Part 3, 2022.

[34] J. Zhao, S. Xiong, J. Ai, J. Wu, L. Z. Huang, and W. Yin, "Stabilized green rusts for aqueous Cr(VI) removal: fast kinetics, high iron utilization rate and anti-acidification," *Chemosphere*, vol. 262, article 127853, 2021.

[35] J. Li, X. Li, S. Ma et al., "Comparing the influence of humic/fulvic acid and tannic acid on Cr(VI) adsorption onto polystyrene microplastics: evidence for the formation of $Cr(OH)_3$ colloids," *Chemosphere*, vol. 307, article 135697, 2022.

[36] U. Schwertmann and R. M. Cornell, *Iron Oxides in the Laboratory: Preparation and Characterization [M]*, John Wiley & Sons, 2008.

[37] K.-Y. Chen, T.-Y. Chen, Y.-T. Chan et al., "Stabilization of natural organic matter by short-range-order iron hydroxides," *Environmental Science & Technology*, vol. 50, no. 23, pp. 12612–12620, 2016.

[38] S. Hu, H. Zhang, Y. Yang et al., "Reductive sequestration of Cr(VI) and immobilization of C during the microbially mediated transformation of Ferrihydrite-Cr(VI)-fulvic acid coprecipitates," *Environmental Science & Technology*, vol. 57, no. 22, pp. 8323–8334, 2023.

[39] C. Chen, J. J. Dynes, J. Wang, and D. L. Sparks, "Properties of Fe-organic matter associations via coprecipitation versus

adsorption," *Environmental Science & Technology*, vol. 48, no. 23, pp. 13751–13759, 2014.

[40] X. Xia, J. Wang, Y. Hu et al., "Molecular insights into roles of dissolved organic matter in Cr(III) immobilization by coprecipitation with Fe(III) probed by STXM-Ptychography and XANES spectroscopy," *Environmental Science & Technology*, vol. 56, no. 4, pp. 2432–2442, 2022.

[41] L. Pontoni, M. Race, E. D. van Hullebusch, M. Fabbricino, G. Esposito, and F. Pirozzi, "Effect of sodium concentration on mobilization and fate of trace metals in standard OECD soil," *Environmental Pollution*, vol. 250, pp. 839–848, 2019.

[42] H. Du, Q. Huang, M. Lei, and B. Tie, "Sorption of Pb(II) by nanosized ferrihydrite organo-mineral composites formed by adsorption versus coprecipitation," *ACS Earth and Space Chemistry*, vol. 2, no. 6, pp. 556–564, 2018.

[43] D. Kim and V. H. Grassian, "Attenuated total reflection-Fourier transform infrared and atomic force microscopy-infrared spectroscopic investigation of Suwannee River fulvic acid and its interactions with α-FeOOH," *ACS Earth and Space Chemistry*, vol. 6, no. 1, pp. 81–89, 2022.

[44] Z. Zhang, W. Shi, H. Ma et al., "Binding mechanism between fulvic acid and heavy metals: integrated interpretation of binding experiments, fraction characterizations, and models," *Water, Air, & Soil Pollution*, vol. 231, no. 4, p. 184, 2020.

[45] Y. Zhang, J. B. Fein, Q. Yu et al., "Surface complexation modeling of the effects of dissolved inorganic carbon on adsorption of U(VI) onto Fe_3O_4 nanoparticles coated with lignite humic acid," *Colloids and Surfaces A: Physicochemical and Engineering Aspects*, vol. 629, article 127260, 2021.

[46] Y. Yang, R. Zhu, Q. Chen et al., "A novel multifunctional adsorbent synthesized by modifying acidified organo- montmorillonite with iron hydroxides," *Applied Clay Science*, vol. 185, article 105420, 2020.

[47] D. Kong, L. He, H. Li, F. zhang, and Z. Song, "Preparation and characterization of graphene oxide/chitosan composite aerogel with high adsorption performance for Cr(VI) by a new cross-linking route," *Colloids and Surfaces A: Physicochemical and Engineering Aspects*, vol. 625, article 126832, 2021.

[48] J. C. Bullen, S. Saleesongsom, K. Gallagher, and D. J. Weiss, "A revised pseudo-second-order kinetic model for adsorption, sensitive to changes in adsorbate and adsorbent concentrations," *Langmuir*, vol. 37, no. 10, pp. 3189–3201, 2021.

[49] Y. Zhou, X. Zhang, H. Zhang et al., "On the removal of the Cr(VI) in water by an ordered mesoporous carbon material: kinetic and isotherm studies," *Water, Air, & Soil Pollution*, vol. 231, no. 2, p. 78, 2020.

[50] Z. Xu, X. Xu, Y. Zhang, Y. Yu, and X. Cao, "Pyrolysis-temperature depended electron donating and mediating mechanisms of biochar for Cr(VI) reduction," *Journal of Hazardous Materials*, vol. 388, article 121794, 2020.

[51] X. Xu, D. Zhu, X. Wang et al., "Transformation of polyvinyl chloride (PVC) into a versatile and efficient adsorbent of Cu(II) cations and Cr(VI) anions through hydrothermal treatment and sulfonation," *Journal of Hazardous Materials*, vol. 423, article 126973, Part A, 2022.

[52] J. Zhang, L. Xie, Q. Ma et al., "Ball milling enhanced Cr(VI) removal of zero-valent iron biochar composites: functional groups response and dominant reduction species," *Chemosphere*, vol. 311, article 137174, Part 2, 2023.

[53] H. Zou, J. Zhao, F. He et al., "Ball milling biochar iron oxide composites for the removal of chromium (Cr(VI)) from water: Performance and mechanisms," *Journal of Hazardous Materials*, vol. 413, article 125252, 2021.

[54] R. He, X. Yuan, Z. Huang et al., "Activated biochar with iron-loading and its application in removing Cr (VI) from aqueous solution," *Colloids and Surfaces A: Physicochemical and Engineering Aspects*, vol. 579, article 123642, 2019.

[55] Y. Zhang, J. B. Fein, Y. Li, Q. Yu, B. Zu, and C. Zheng, "U(VI) adsorption to Fe_3O_4 nanoparticles coated with lignite humic acid: Experimental measurements and surface complexation modeling," *Colloids and Surfaces A: Physicochemical and Engineering Aspects*, vol. 614, article 126150, 2021.

[56] P. Miretzky and A. F. Cirelli, "Cr(VI) and Cr(III) removal from aqueous solution by raw and modified lignocellulosic materials: a review," *Journal of Hazardous Materials*, vol. 180, no. 1–3, pp. 1–19, 2010.

[57] Z. Ai, Y. Cheng, L. Zhang, and J. Qiu, "Efficient removal of Cr(VI) from aqueous solution with Fe@Fe2O3Core–shell nanowires," *Environmental Science & Technology*, vol. 42, no. 18, pp. 6955–6960, 2008.

[58] J. Tang, B. Zhao, H. Lyu, and D. Li, "Development of a novel pyrite/biochar composite (BM- FeS_2@BC) by ball milling for aqueous Cr(VI) removal and its mechanisms," *Journal of Hazardous Materials*, vol. 413, article 125415, 2021.